RESEARCH TRIANGLE INSTITUTE

RTI/3629/90-Quarterly September 1990

SEMICONDUCTOR DIAMOND TECHNOLOGY

Quarterly Report -- Second Quarter
1 April 1990 - 30 June 1990

R. J. Markunas
R. A. Rudder
J. B. Posthill
R. E. Thomas

STRATEGIC DEFENSE INITIATIVE ORGANIZATION
Innovative Science and Technology Office

Office of Naval Research
Program No.
N00014-86-C-0460

POST OFFICE BOX 12194 RESEARCH TRIANGLE PARK, NORTH CAROLINA 27709-2194

REPORT DOCUMENTATION PAGE

Form Approved
OMB No 0704-0188

1. AGENCY USE ONLY *(Leave blank)*	2. REPORT DATE	3. REPORT TYPE AND DATES COVERED
	1 November 1990	Quarterly Report, 1 April 1990 - 30 June 1990

4. TITLE AND SUBTITLE

Semiconductor Diamond Technology

5. FUNDING NUMBERS

N00014-86-C-0460

6. AUTHOR(S)

R.J. Markunas, R. A. Rudder, J. B. Posthill, R. E. Thomas

7. PERFORMING ORGANIZATION NAME(S) AND ADDRESS(ES)

Research Triangle Institute
P. O. Box 12194
Resarch Triangle Park, NC 27709

8. PERFORMING ORGANIZATION REPORT NUMBER

83U-3629

9. SPONSORING/MONITORING AGENCY NAME(S) AND ADDRESS(ES)

Office of Naval Research
800 N. Quincy Street
Arlington, VA 22217-5000

10. SPONSORING/MONITORING AGENCY REPORT NUMBER

11. SUPPLEMENTARY NOTES

12a. DISTRIBUTION/AVAILABILITY STATEMENT

Approved for public release; unlimited distribution

12b. DISTRIBUTION CODE

13. ABSTRACT *(Maximum 200 words)*

Semiconducting diamond technology development this quarter has focussed on: (1) metal substrate development by the formatin of ultra-thin refractory metal layers on Ni(100) surfaces, (2) advancement toward ALE by obtaining absorption/desorption data from Si(100) surfaces for hydrogen and halogen species in the surface chemistry facility, (3) continuing development of low pressure rf-plasma assisted diamond CVD for diamond device fabrication. A diamond FET fabrication sequence that utilizes selective area epitaxy of doped diamond on an insulating diamond single crystal substrate is proposed. This process sequence takes advantage of (1) well-established lithography and etching processes for mask materials, (2) the fact that diamond is difficult to nucleate on most materials that could be used as a masking layer, and (3) the established capability of depositing gate-quality dielectrics by RPECVD.

Selective area diamond homoepitaxy has been demonstrated through lithographically defined windows in Si and Ni masking layers. Additionally, diamond is observed to overgrow (epitaxiall and laterally) the Si masking layer at approximately the same rate as the vertical epitaxy.

Doping studies have included Li, Na, and B incorporation during growth. All doped samples were observed to be p-type. An activation energy of 0.23eV for Li doping was confirmed with a room temperature mobility of 143 cm^2-$V^{-1}sec^{-1}$, and activation energies of 0.24eV for $T > 125^oC$ and 0.006eV for lower temperatures were measured for B doping.

14. SUBJECT TERMS

15. NUMBER OF PAGES

16. PRICE CODE

17. SECURITY CLASSIFICATION OF REPORT	18. SECURITY CLASSIFICATION OF THIS PAGE	19. SECURITY CLASSIFICATION OF ABSTRACT	20. LIMITATION OF ABSTRACT

TABLE OF CONTENTS

LIST OF FIGURES

1.0 Introduction

This is the 1990 Second Quarterly Report on the Semiconducting Diamond Program Contract No. N00014-86-C-0460 at Research Triangle Institute.

A low pressure rf-plasma assisted CVD system routinely deposits high quality polycrystalline or homoepitaxial layers. Last quarter, emission and mass spectroscopy were used to better characterize the growth conditions for diamond deposition in this technique. The plasma was seen to be a chemically reactive plasma creating atomic hydrogen, converting CH_4 into C_2H_2, and gasifying graphite or other solid carbon sources into C_2H_2. The effective temperature of the plasma varies between 3200K and 3420K, depending on the pressure and power conditions. This quarter, work in the low pressure rf-plasma assisted CVD system has investigated doping and selective growth techniques necessary for diamond device development.

Li and Na were investigated as possible n-type dopants in diamond. N-type behavior was not observed on any homoepitaxial films. Some polycrystalline films doped with Li appeared n-type from Seeback measurements. However, homoepitaxial layers doped with Li appeared p-type from Hall measurements. Proof of carrier type in a polycrystalline material from Seeback effect may not be conclusive. Electrons may diffuse more rapidly through grain boundaries than holes could diffuse, giving a p-type sample the appearance of being n-type. Na was not investigated extensively as a dopant source due to reactions of the activated Na with the feedthroughs in the chamber. Leaks developed soon after NaOH was introduced into the reactor. Elimination of residual Na from the reactor involved rebuilding the heater stage and

replacement of the plasma tube. Late this quarter, B_2H_6 was installed on the reactor to provide a controlled source of B for doping studies. Doping levels of 10^{17} cm^{-3} were obtained with a 1000 ppm source of B_2H_6 in H_2.

Selective area homoepitaxial deposition and overgrowths were performed this quarter in the low pressure rf-plasma system. Deposits of Ni and Si on natural diamond substrates provided deposition masks preventing diamond deposition except on areas where the Ni or Si had been etch removed. Ni masks were observed to separate allowing diamond growth on areas other than the windows in the Ni that had been lithographically defined. Selective area growth and overgrowth of Si patterned areas was observed. The overgrowth appeared nearly isotropic with the diamond growing as far above the Si mask as it did across the Si mask. Micro-Raman was used to examine the quality of the diamond deposited in the window, outside the window where some nucleation on Si was observed, and along the overgrowth.

Surface chemistry studies this quarter began to investigate the interactions of molecular halogens with clean or hydrogen passivated surfaces. Last quarter, improvements in the geometry of the thermal mass desorption stage made dramatic improvements in the mass desorption signal. The β_1 and β_2 desorption peaks from a Si(100):H surface are clearly distinguished from the hydrogen background in the chamber. LEED measurements in conjunction with the mass desorption spectrum confirmed previous work by others about the nature of the β_1 and β_2 bonding configurations. Through controlled dosing, one is able to control the surface state of the Si surface from an atomically clean Si(100) 2×1 surface to a hydrogen terminated Si(100) 2×1

:H surface to a completely hydrogenated surface Si(100) 1×1:H. The chemical reactivity of the Si surface will depend on the state of the surface termination. This quarter, clean and hydrogen passivated surfaces have been dosed with molecular F_2 and Cl_2. Desorptions from chlorinated and fluorinated Si surfaces have shown the desorption product to be Si-bearing, not F_2 or Cl_2. Furthermore, chemical extraction of fluorine and chlorine from Si surfaces has been demonstrated using atomic hydrogen. While the extraction products have not yet been determined, the extraction process was been observed for temperatures from 25 to 500 ° C.

2.0 Metal Substrate Development and Heteronucleation Studies

Research in a previous phase of this program has already demonstrated the ability to prepare and polish Ni single crystals for subsequent growth of epitaxial metal layers. Additionally, molecular beam epitaxy (MBE) has been used to grow Ni_xCu_{1-x} epitaxial films of different compositions and, hence, lattice parameters. As the Ni and Cu lattice parameters straddle the lattice parameter of diamond, this approach to substrate development for diamond heteroepitaxy was utilized to engineer an exact lattice match with the diamond [$a_o(Ni_{0.82}Cu_{0.18}) \simeq 3.567$ Å $\simeq a_o$(Diamond) at T=700 ° C]. This capability already exists.

Substrate development in this quarter has built upon the available metals MBE expertise by investigating the modification of surface chemistry while maintaining near-lattice-matching to diamond. In particular, the deposition of Mo onto Ni(100) was explored. The technical approach for this was to deposit an ultra thin layer of a highly reactive refractory metal (strong carbide forming element) on a Ni(100) surface

that would be epitaxial and, possibly, pseudomorphic. Although bulk Mo is body-centered cubic with a lattice parameter of a_o(Mo) = 3.1463Å, the potential still exists to modify the surface of a Ni(100) crystal chemistry while maintaining near lattice matching to diamond. There is a partial analogy for this phenomenon in the Fe on Cu(100) system. Deposition of ultrathin layers of Fe on Cu(100) will result in a layer of metastable, pseudomorphic, face-centered cubic phase of Fe (γ-Fe) being created. It is anticipated that the modification of the surface chemistry of the Ni(100) substrate will alter the heteronucleation behavior of CVD diamond - potentially leading to heteroepitaxy.

The Mo/Ni(100) work was performed at RTI in collaboration with Professor K.J. Bachmann and his graduate student, Y.-H. Lee, of North Carolina State University. The Ni(100) substrates used in this study were received with diamond turned surfaces and polished using 9μm, 5μm alumina slurry followed by 2 hours of polishing in a colloidal silica solution. The substrates were then given a solvent clean of TCE, acetone and methanol followed by etching in an H_2O-based 15% nitric acid solution. After a deionized water rinse and N_2 blow dry, the samples were loaded into the sample preparation chamber of the MBE system. They were then subjected to Ar^+ sputter cleaning under the following conditions: Ar pressure of 10^{-5} Torr in the ion gun chamber and 10^{-7} Torr in the sample chamber; a discharge voltage of 40V and a filament current of 6A; a beam voltage of 500V and accelerating voltage of 100V. This established a sputter rate of 20Å- sec^{-1}. The sputter time was typically 40 min. The sputtered samples were then annealed at $\sim$ 600 °C for 60 min. After cleaning by

sputtering/annealing, the AES and XPS spectra show no presence of O, but persistent trace levels of C. LEED studies of the in vacuo cleaned Ni substrates show typically sharp Ni(100) 1 $\times$ 1 patterns. The samples were then transferred to the metal MBE growth chamber of the integrated processing facility. The system provided for two separately controlled and shuttered e-beam hearths. The chamber is pumped by two cryogenics CT-8 Pumps and is able to attain base pressures in the 10^{-11} Torr range while growth pressures are typically in the 10^{-9} Torr range. The growth rate was controlled by a quartz crystal oscillator and was typically 0.2 Å- sec^{-1}. The samples were characterized without breaking vacuum by LEED, XPS, and AES. After these measurements, the samples were removed from the vacuum system and examined by SEM and XRD.

The variation of the AES intensities with increasing film thickness has been used to determine the mode of growth at 200 ° C. The AES technique was performed in a UHV surface analysis system equipped with a hemispherical electron energy analyzer (operated in constant pass energy mode) and an Auger electron gun. Figure 1 shows the first derivative Auger intensities of the Mo MNN (186eV) and Ni LMM (61eV) transitions from the Mo/Ni(100) surface as a function of Mo film thickness. The exponential intensity indicates a layer by layer growth mechanism. Only a diffuse, incomplete LEED pattern was observed for these films. Thicker layers of Mo($>$ 500Å) and Mo-Ni multilayers of 20Å period deposited at 200 ° C resulted in well-defined X-ray diffraction peaks, indicating that films grown at this temperature are crystalline.

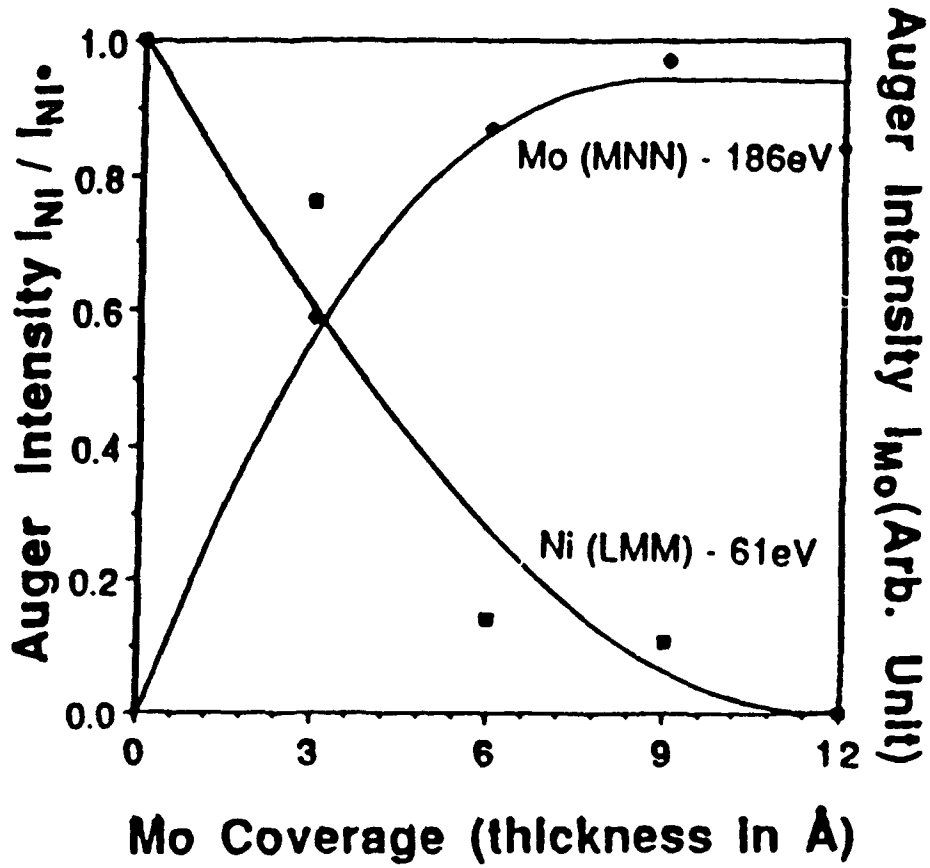

Figure 1. Intensity Variations of AES for the Mo MNN (186eV) and Ni LMM (61eV) peaks as a function of Mo Coverage.

In order to obtain an epitaxial relationship between the deposited Mo films and the Ni substrate, the growth temperature was increased. Growth of ultrathin ($\sim$ 20Å) Mo on Ni(100) resulted in a well-defined LEED pattern at 550 ° C. These patterns are similar to the diffraction pattern of the Ni(100) substrate. The same tendency was observed for a thicker film ($\sim$ 250Å Mo). However, AES of Mo films of up to 500Å thickness grown at 550 ° C on Ni(100) clearly show the Ni LMM (61eV) transition which has a very low escape depth ($<$ 10Å). The source of this phenomenon could be: (a) incomplete coverage, (b) intermetallic or alloy formation during growth, or (c) a persistent thin Ni coverage on the growing Mo film. SEM reveals that the growth morphology is clearly 3-dimensional which is shown in Figure 2a at a 45 ° viewing angle. High-resolution AES (HRAES) measurements utilizing an electron beam current of $\sim$ 0.8nA at a beam size of $\sim$0.1μm diameter reveal bare Ni channels in between the 3-dimensional Mo deposit. Therefore, Mo films grow at T $\sim$ 550 ° C by the Volmer-Weber mechanism. HRAES data taken while focusing on the surface of a Mo island still shows the presence of Ni LMM (61eV and 848eV) signals. However, after brief sputtering ($<$ 15Å) these signals vanish, restoring a clean Mo surface. This excludes intermetallic/alloy formation during growth with the possible exception of the Mo/Ni interfacial region. Therefore, the source of the Ni LMM peaks on the as-grown surface of the Mo islands is the coverage of these islands by Ni atoms during all stages of nucleation and growth processes.

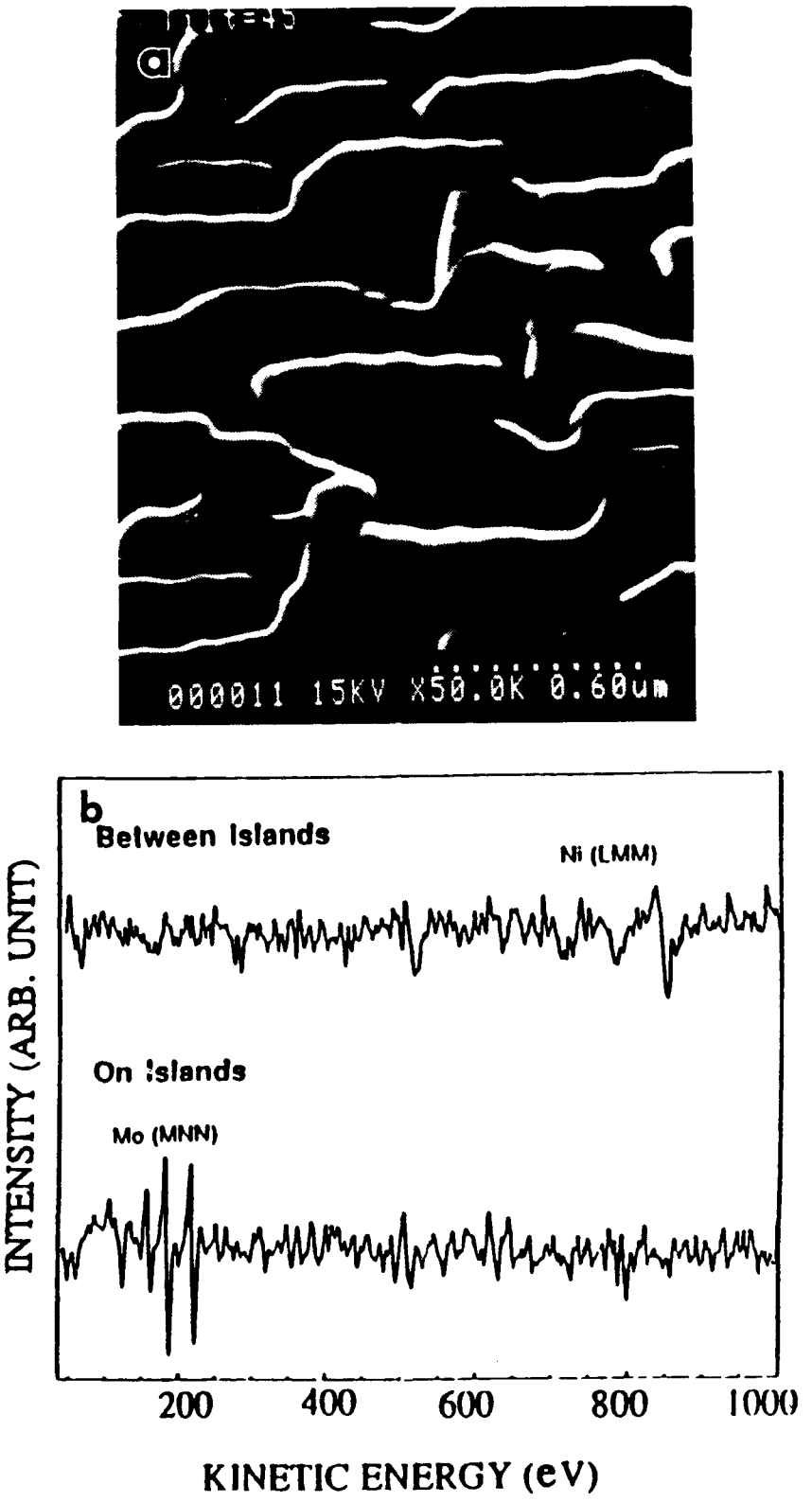

Figure 2. (a) SEM micrograph of Mo (250 Å) islands on Ni(100) grown at 550 ° C at 45 ° viewing angle; (b) Corresponding HRAES of the sample, both on and between the islands.

In order to determine whether the surface order of the ultrathin ($\sim$ 20Å) Mo layers on Ni(100) grown at 200 ° C can be improved by annealing, samples were annealed for 10 min. at temperatures from 250 ° C up to 450 ° C in 50 ° C increments, adding a final annealing step at 550 ° C. The variations of Ni substrate peak intensity as a function of annealing temperatures are shown in Figure 3. There is a large increase in the Ni intensity after 550 ° C annealing while the intensity variations of the Mo MNN (186eV) Auger peak show an opposite trend. This indicates an onset of interdiffusion at this temperature. The magnitude of the intensity of the Mo MNN (186eV) peak was about the same as that of Ni LMM (848eV) after annealing - indicating that there is still a substantial Mo concentration in the near-surface region. LEED examination showed no well-defined pattern immediately after Mo deposition and after annealing as high as 450 ° C. However, after 550 ° C annealing of a 20Å Mo film on Ni, a different diffraction pattern of the reconstructed surface appears. This is shown in Figure 4.

Since the free energies of the Mo and Ni surfaces are estimated to be 2463 erg-cm^{-2} and 2072 erg-cm^{-2}, respectively, and there exists a substantial lattice mismatch. it might be expected that Mo grows on Ni by either a Stranski-Krastnov or Volmer-Weber mechanism. This is indeed the case for high temperature (550 ° C) deposition of Mo on Ni(100). At sufficiently low temperature, the sticking coefficient of the impinging Mo atoms approaches unity, irrespective of the matching to the underlying lattice. eliminating discrimination between a foreign substrate and the Mo-covered parts of the surface. Thus, low temperature deposition results in uniform coverage, but

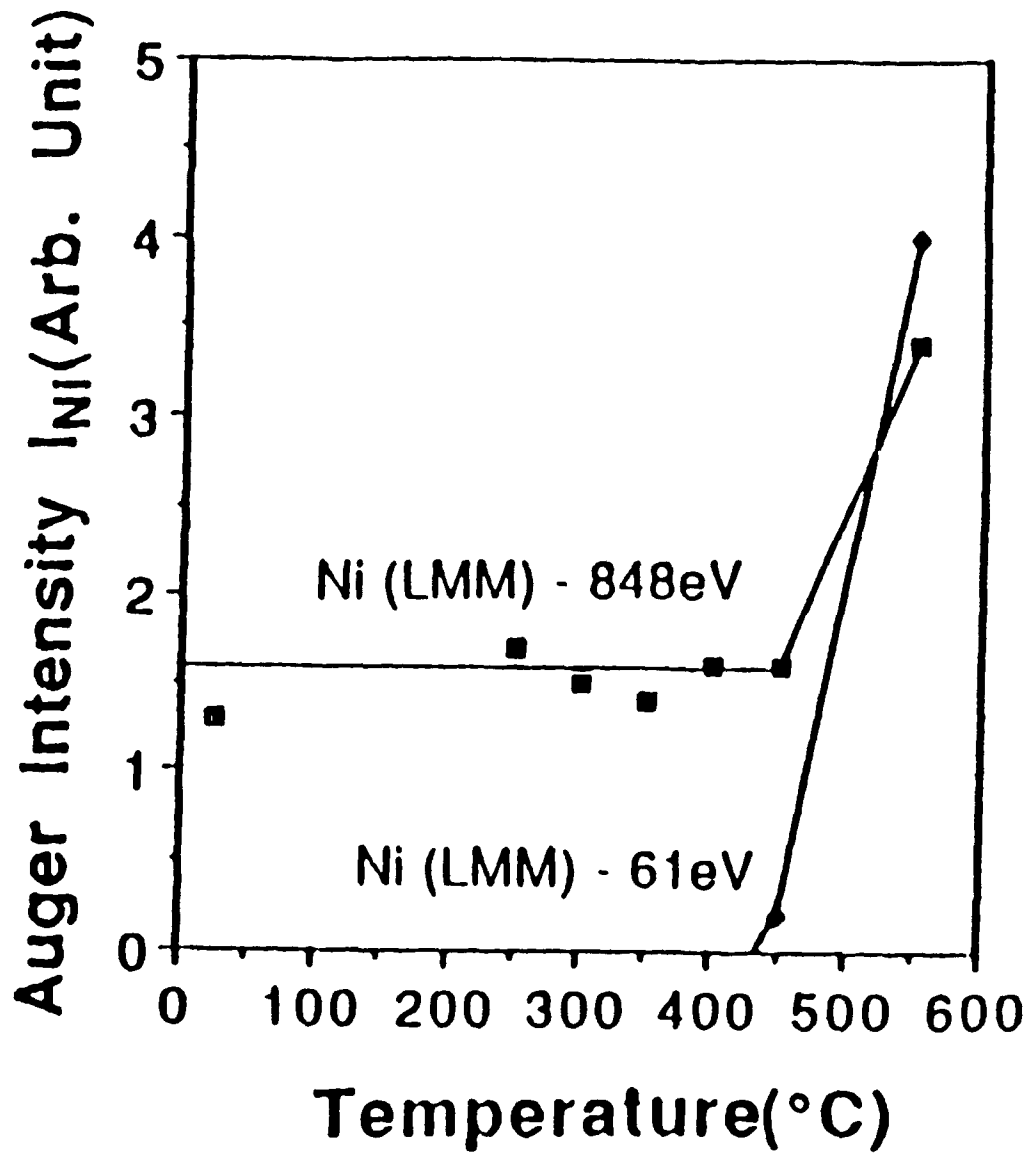

Figure 3. Intensity variations of AES for the Ni LMM (848eV) and Ni LMM (61eV) signal as a function of annealing temperature.

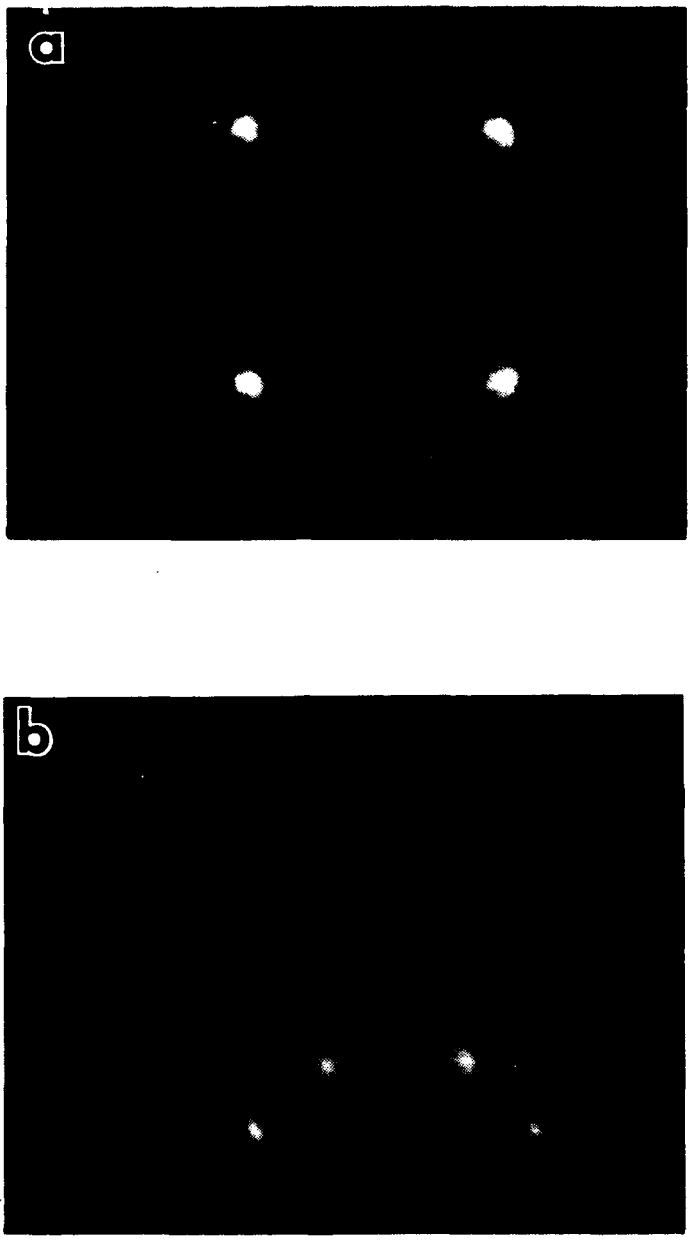

Figure 4. LEED patterns of: (a) clean Ni(100) substrate (electron energy=157.8eV); (b) Mo (20Å) on Ni(100) grown at 200 ° C, annealed at 500 ° C (electron energy=148eV).

not necessarily epitaxy. Upon heating to a critical temperature range, where the barrier to interdiffusion/interface reaction can be overcome, the Mo overlayer rearranges under incorporation of Ni. In view of the small thickness (20 Å) of the film, the determination of the atomic fraction of Ni in this film is difficult and no accurate quantitative information can be given at present about the chemical composition. However, the LEED pattern clearly shows doubling of the surface unit cell for the annealed film. This surface-modified Ni(100) crystal is certainly unique and attempting diamond nucleation and growth on this surface warrants exploration.

In summary, the growth of thin Mo layers on Ni(100) and multilayer Mo-Ni heterostructures has been investigated. At 200 °C, polycrystalline, uniform, and topographically featureless Mo on Ni(100) films are formed. In contract, growth of Mo on Ni(100) at 550 °C proceeds by the Volmer-Weber mechanism. Finally, annealing experiments performed on Mo/Ni(100) heterostructures deposited at 200 °C, show an onset of interdiffusion at ~550 °C and, simultaneously, a unique reconstruction of the surface.

Attempts were made to grow diamond on a Mo-terminated Ni(100) crystal. An ultrathin layer (~ 20 Å) of Mo was grown on Ni(100) at 200 °C by MBE using the method described above. Based on results described above, it was believed that once the Mo/Ni(100) structure was raised to the diamond growth temperature of $\geq$ 600 °C, interdiffusion would create a surface structure and chemistry similar to that observed previously. Due to the need to perform other tasks on this program, the diamond reactor on the integrated processing system was not available for in-vacuo transfer of

the Mo/Ni(100) substrate to a diamond CVD system. Hence, an air transfer was utilized. The PECVD diamond growth was done at a temperature of $\sim$ 600 °C; using a mixture of CO, CH_4, and H_2; at a pressure of 1 Torr. Figure 5 shows SEM results from this run. Notice the difference in the diamond nucleation density between the Mo/Ni(100) region and the "bare" Ni(100) region; (this region did not receive Mo deposition because it was under the mask). Somewhat surprisingly, the nucleation density of diamond is substantially greater on the "bare" Ni(100) surface. Although this appears to suggest that an ultra-thin Mo interlayer does not promote diamond nucleation, we are of the opinion that this experiment is not definitive. It is most probable that all the $\sim$ 20 Å Mo was oxidized during the air transfer to the diamond reactor. Hence, this experience has lead us to conclude that it is no longer appropriate to continue work with only one of the diamond reactors integrated with the other UHV processing and analytical systems. Plans are underway to attach the second, high-power PECVD diamond reactor to the RTI integrated processing system so as to be able to carry out more controlled surface modifications in order to promote diamond heteroepitaxy.

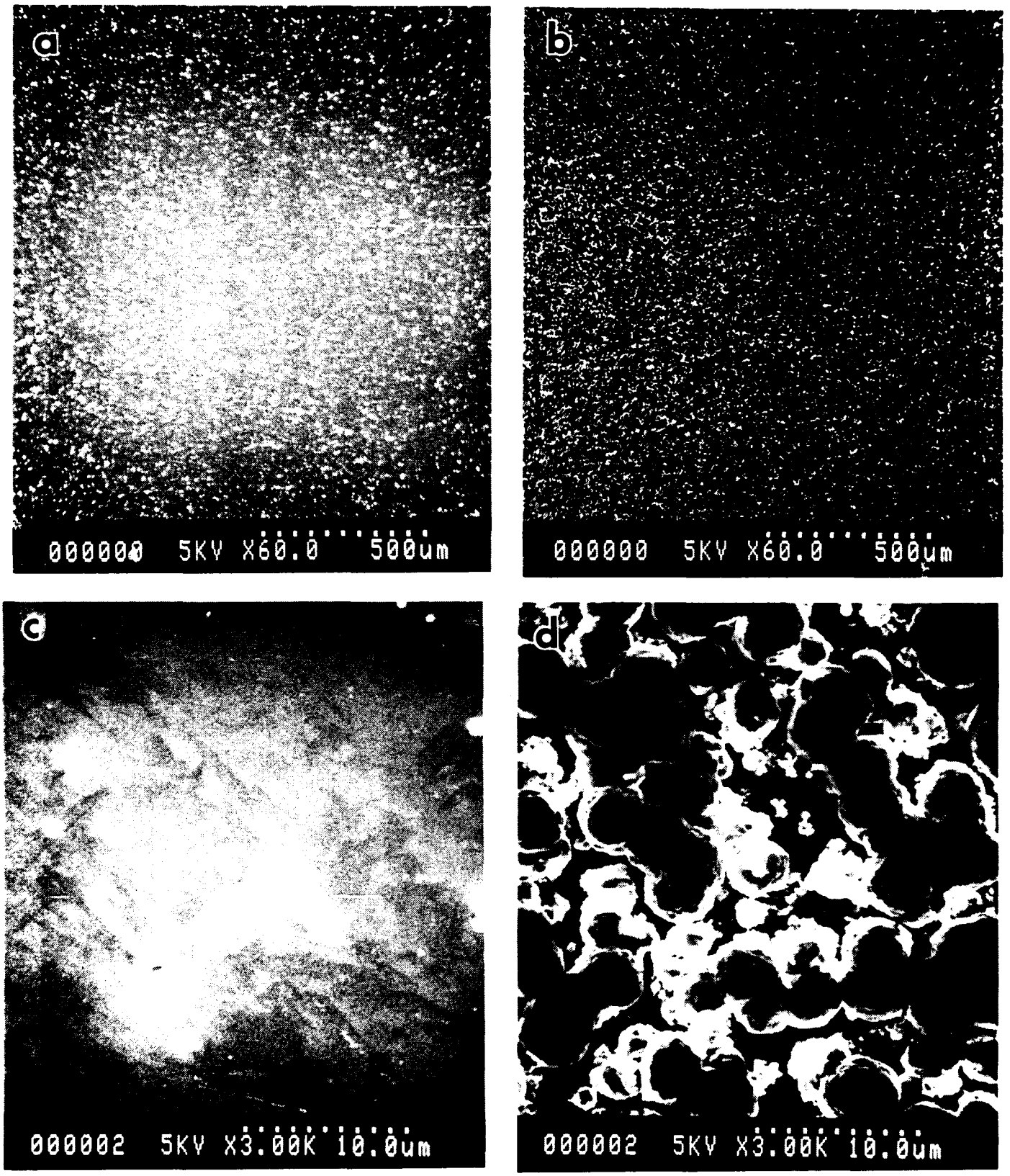

Figure 5. SEM micrographs from diamond deposition on Mo/Ni(100) heterostructure: (a & b) low magnification comparing Mo-terminated region with bare Ni; (c & d) higher magnification comparing Mo-terminated region with bare Ni.

3.0 Surface Chemistry Studies

Clean Si(100) 2 $\times$ 1 surfaces have been exposed to atomic hydrogen, molecular fluorine, and molecular chlorine. The samples were ramped in temperature until desorption products were detected by the mass quadrupole. For atomic hydrogen exposure, hydrogen desorption was observed with peaks in the desorption spectrum at 420 and 540 ° C. Desorption products such as SiH_x were not observed. For chlorine and fluorine dosing, the silicon surface was dosed with approximately 1 monolayer of either chlorine or fluorine and the sample was ramped up in temperature to determine desorption products and temperatures. In the case of fluorine on silicon we find that SiF_2 and SiF_4 are desorbed at a temperature of approximately 560 ° C for a heating rate of 5 ° C/sec. Figure 6 shows the desorption spectrum obtained for the heating rate of 5 ° C/sec. This is quite close to a literature value of 530 ° C for a heating rate of 4 ° C/sec. For chlorine on silicon desorption products consist of $SiCl_2$ and $SiCl_4$ and are desorbed at a temperature of approximately 670 ° C with a linear heating rate of 5 ° C/sec. Figure 7 shows the desorption spectrum of $SiCl_2$.

The next experiment was to dose a clean, reconstructed Si(100) surface with either fluorine or chlorine and dose a second time with either atomic or diatomic hydrogen. After dosing the sample was again ramped up in temperature. In short we find that atomic hydrogen will strip halogens off of the silicon (100) surface and diatomic hydrogen will not. Furthermore, we find that halogens are ineffective at removing hydrogen from the silicon surface. Note that in these experiments diatomic halogen species were used to dose the surface. It is expected that atomic halogens would be more effective

at removing hydrogen from the silicon surface, but we expect that the reaction would not be self-limiting, and a continuous etching of the silicon substrate would ensue.

We have shown that hydrogen-halogen exchanges occur at room temperature. An ALE growth sequence is likely to be performed at much higher temperatures. In order to assess the efficiency of the exchange process at elevated temperatures, samples were dosed with Cl_2 at room temperature and then dosed at either 25 ° C, 400 ° C, or 600 ° C with hydrogen. The sample was then cooled to room temperature and the thermal desorption spectra taken.

Figure 8 shows the atomic masses monitored during the thermal desorption. The spectra in the viewgraph were taken from a sample that was held at room temperature for both Cl_2, and hydrogen dosing. We see a large hydrogen desorption feature consisting of the β_1 peak at 550 ° C, and β_2 peak at 430 ° C. Two peaks were also seen for Cl and HCl desorption. Given the fact that the Cl and HCl peaks are at the same temperature, it is likely that the Cl seen is a result of fragmentation of HCl in the ionizer. The first HCl desorption peak occurs at 430 ° C, which again makes it likely that the peak is associated with the β_2 hydrogen peak. The second HCl peak is at 600 ° C and appears to arise from a desorption process separate from the β_1 desorption.

We also see a variety of SiH_xCl_y species, all of which desorb at 715 ° C. The simultaneous desorption of species usually indicates the same parent molecule. In this case, the most likely candidate accounting for all the different chlorosilanes seen is $SiHCl_3$.

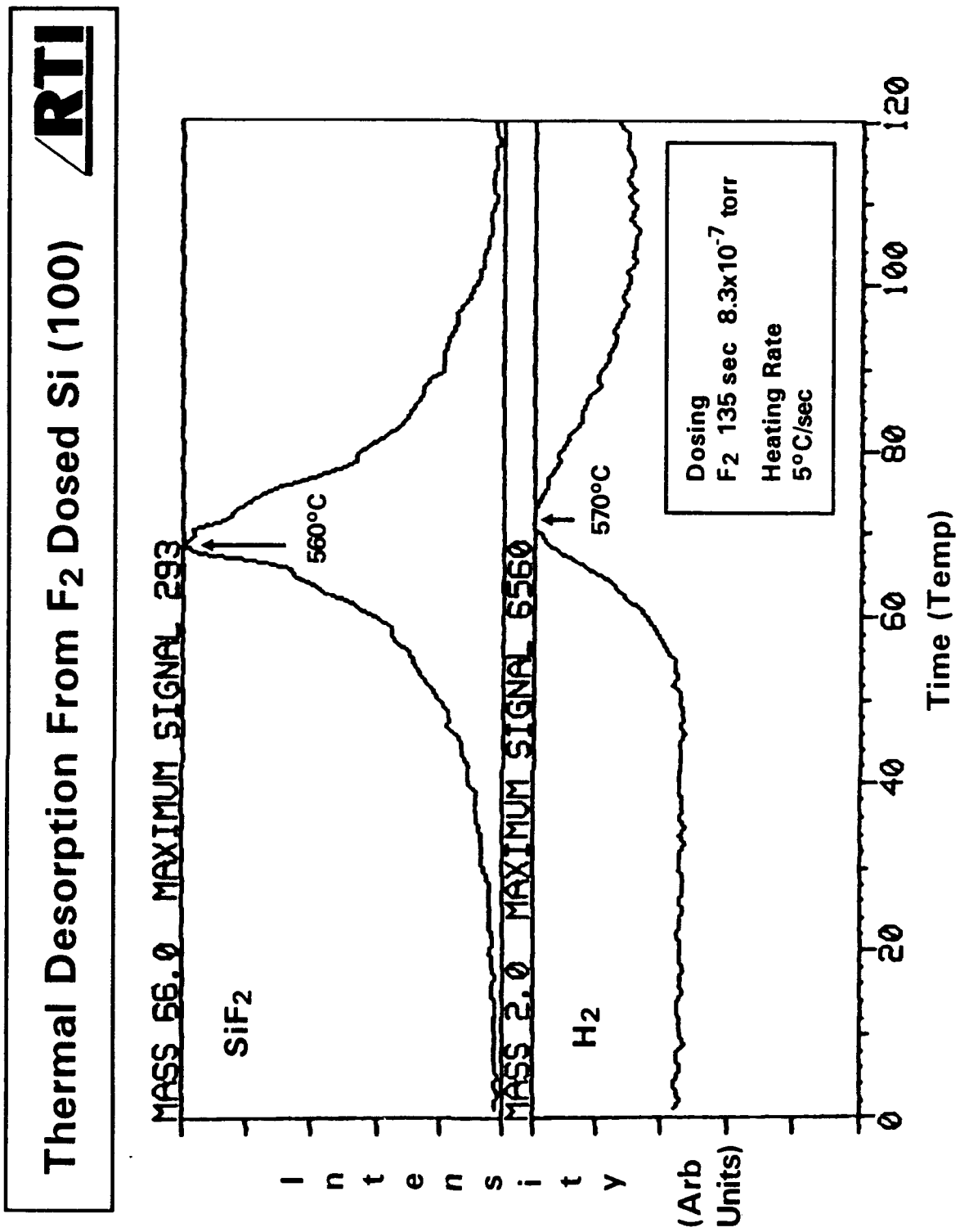

Figure 6. Thermal desorption spectrum from a fluorine dosed Si(100) surface.

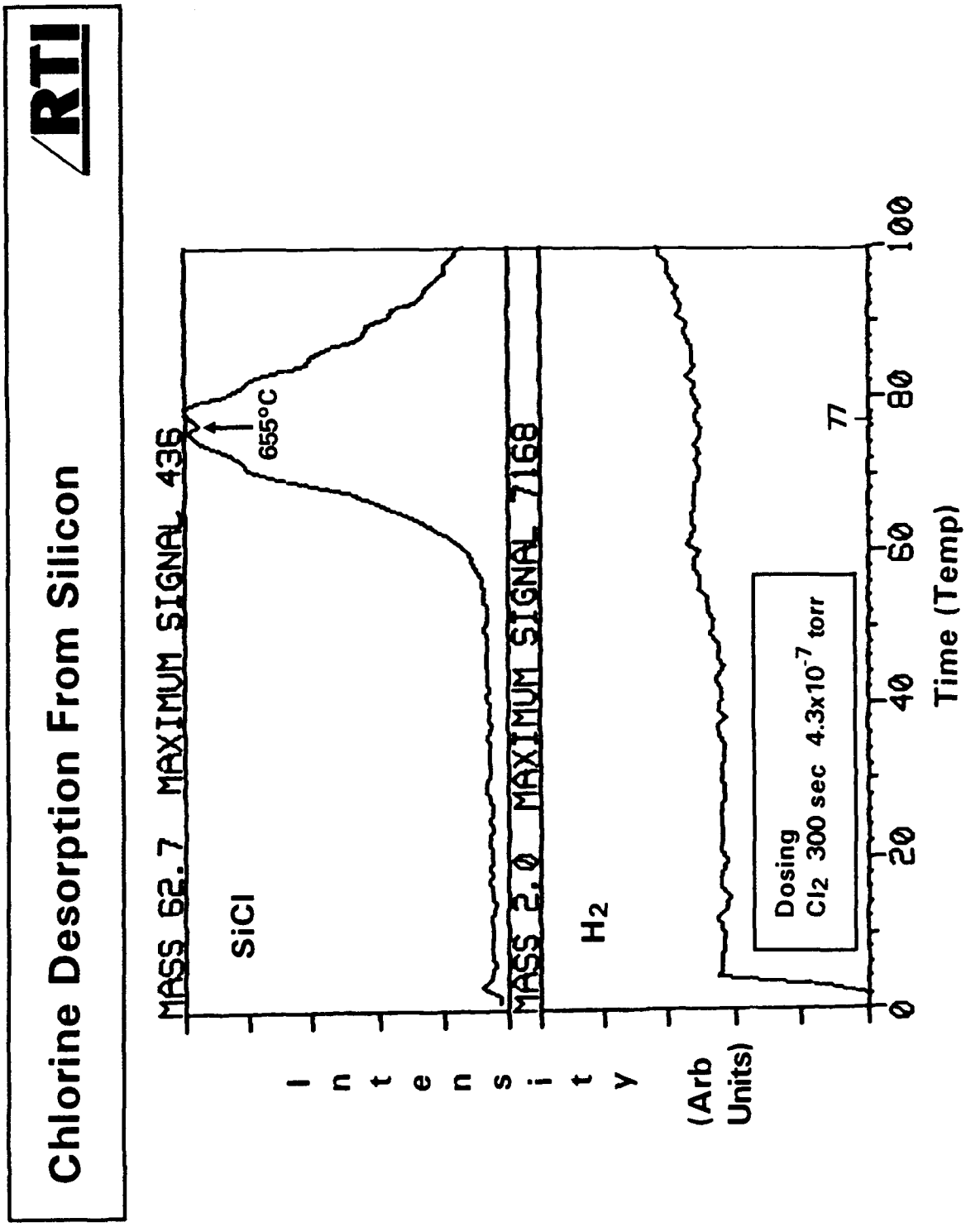

Figure 7. Thermal desorption spectrum from a chlorine dosed Si(100) surface.

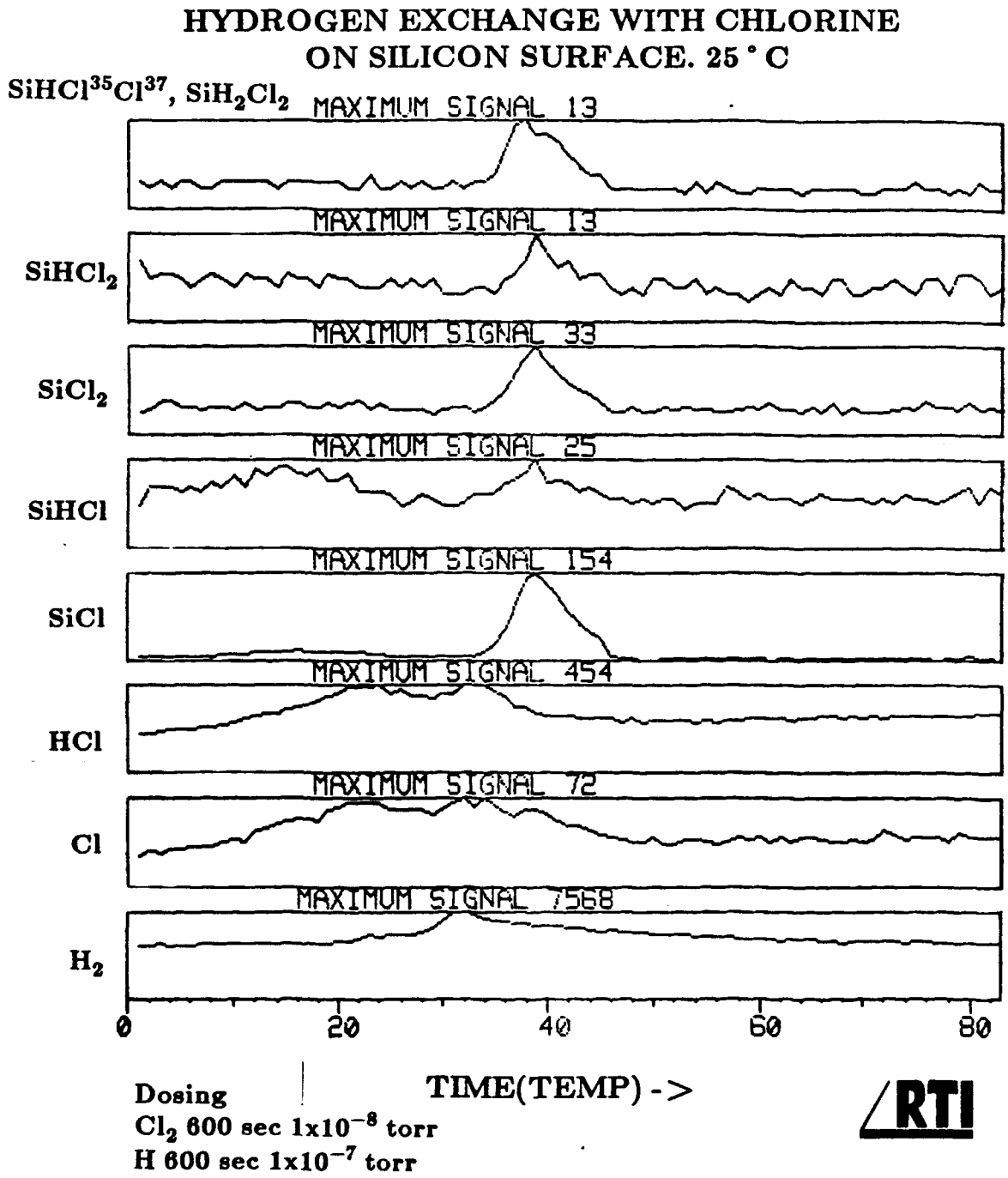

Figure 8. Thermal desorption spectrum from a Si(100) surface that was first dosed with chlorine and then atomic hydrogen. Spectrum shows the masses monitored during a typical desorption experiment.

The next series of figures, 9,10, and 11, follow the evolution of the H_2, HCl, and SiCl peaks, respectively, as a function of substrate temperature during hydrogen dosing. Three different substrate temperatures were used, 25 ° C, 400 ° C, and 600 ° C. The intermediate temperature is at a temperature slightly lower than the first hydrogen desorption temperature. We expect hydrogen to remain on the surface at this temperature after the exchange process. At 600 ° C all of the hydrogen should desorb from the surface during the exchange process.

Figure 9 shows three hydrogen desorption spectra taken after holding the substrate at three different temperatures during hydrogen dosing. The spectrum taken after dosing at 25 ° C shows the typical desorption pattern from silicon with 2 desorption peaks. For the sample held at 400 ° C, the β_2 peak has disappeared and additional hydrogen has been added to the surface. At 600 ° C we begin to see a decrease in the maximum hydrogen desorption peak. It appears that hydrogen is still being added to the surface, but a significant amount is desorbing prior to the temperature ramp to collect the spectrum.

Figure 10 shows the same sample as Figure 9, but in this case, the HCl mass is monitored. At 25 ° C we see 2 desorption peaks, one which appears to be associated with the β_2 hydrogen desorption, and one with an independent desorption of HCl from the silicon. The sample held at 400 ° C during dosing has lost the lower temperature HCl peak, but retains 600 ° C peak. Finally at 600 ° C, both peaks have disappeared.

A more direct measure of the exchange efficiency at elevated temperatures is given in Figure 11 which shows the same samples with the SiCl mass monitored. This

series of data shows two trends: the magnitude of the desorption peak decreases as substrate temperature increases during hydrogen dosing, and the desorption temperature increases as substrate temperature increases.

The exchange process is clearly efficient at elevated temperatures, and could be included as a step in an ALE growth sequence. However, the details of the exchange mechanism are still not clear. Based on a report by Cheung and Coburn[1], we have ruled out etching of the silicon by atomic hydrogen as the removal process. The published work indicates that addition of chlorine to the silicon surface immediately terminates the etching process. If chlorine addition is stopped the hydrogen gradually removes the chlorine and etching of the silicon resumes.

[1] M-C. Cheung, J.W. Coburn, J. Vac. Sci. Tech. A 8, 1969 (1990).

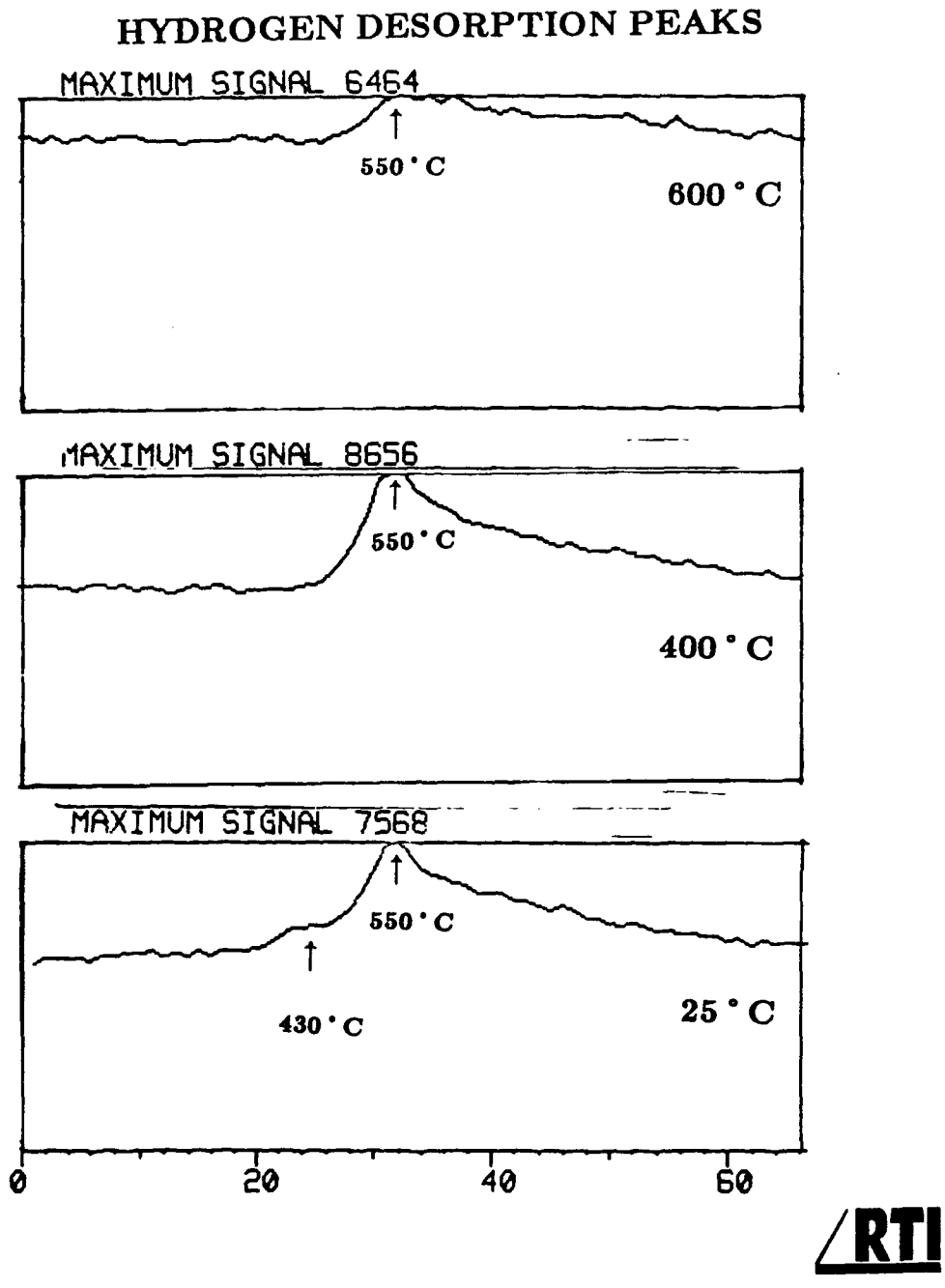

Figure 9. This figure shows thermal desorption spectra of hydrogen as a function of substrate temperature during hydrogen dosing. The samples were dosed with chlorine at room temperature and then with hydrogen at the indicated temperatures. Next the samples were cooled to room temperature and the thermal desorption spectrum taken.

HCl DESORPTION PEAKS

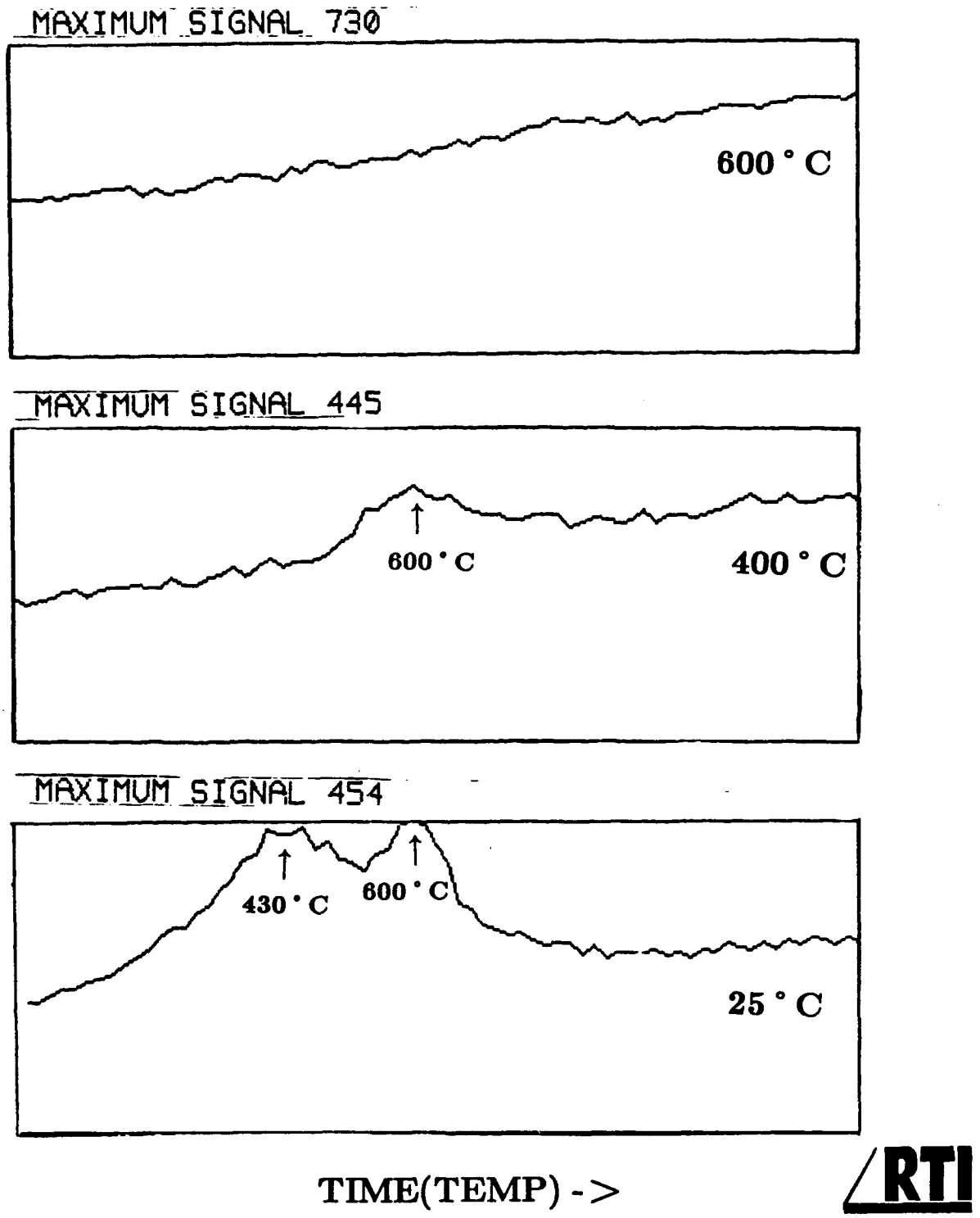

Figure 10. This figure shows thermal desorption spectra of HCl as a function of substrate temperature during hydrogen dosing. The samples were dosed with chlorine at room temperature and then with hydrogen at the indicated temperatures. Next the samples were cooled to room temperature and the thermal desorption spectrum taken.

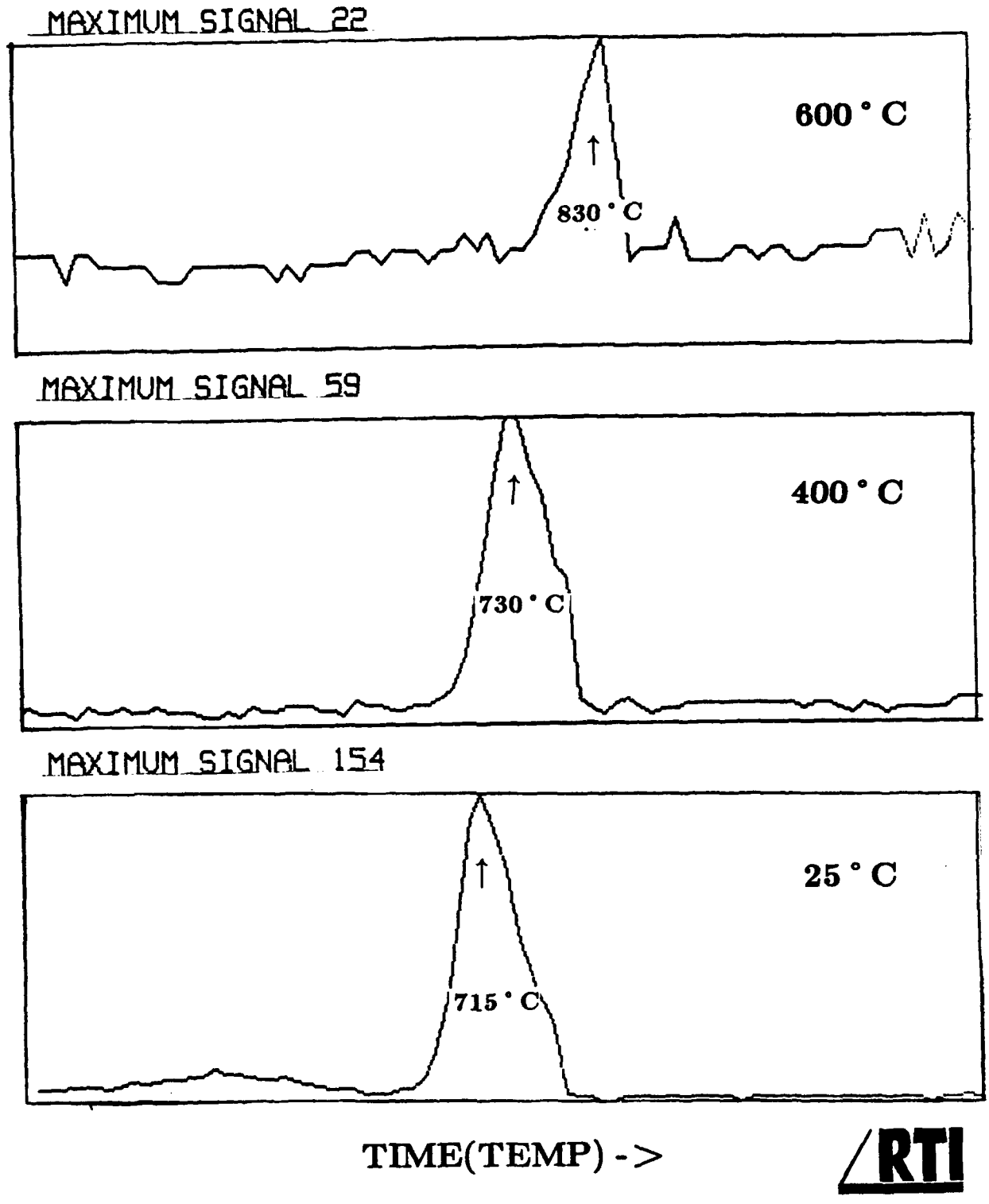

Figure 11. This figure shows thermal desorption spectra of SiCl as a function of substrate temperature during hydrogen dosing. The samples were dosed with chlorine at room temperature and then with hydrogen at the indicated temperatures. Next the samples were cooled to room temperature and the thermal desorption spectrum taken.

4.0 Low Pressure rf-plasma Assisted Diamond CVD

As mentioned in the introductory section, work in the plasma system focused on developing doping and selective growth capabilities. Development of these two techniques will allow fabrication of diamond test structures on natural diamond substrates. Figure 12 shows a schematic of a diamond FET process using selective epitaxy. In that process, silicon and titanium are deposited and photolithographically defined on the substrate. Holes in the titanium layer will act as seeds for doped diamond deposition. The silicon masking layer prevents doped diamond deposition between devices. Following diamond deposition, the silicon will be etch removed. Thus, each device will be electrically isolated from one another. From previous experiments, we expect the formation of a titanium carbide layer upon introduction of the Ti to the H_2/CH_4 plasma. This carbide layer should provide ohmic contact to the doped diamond. Following 2000 - 3000 Å doped diamond deposition, ohmic source/drain contacts and a Schottky gate would be deposited. Alternatively, SiO_2 could be deposited and patterned for source, drain, and gate contacts, then the sample metallized. This fabrication approach uses standard lithographic techniques and patterns standard materials. Thus, without diamond etching, diamond device structures can be fabricated using doping and selective epitaxy technologies.

Diamond FET by Selective Epitaxy

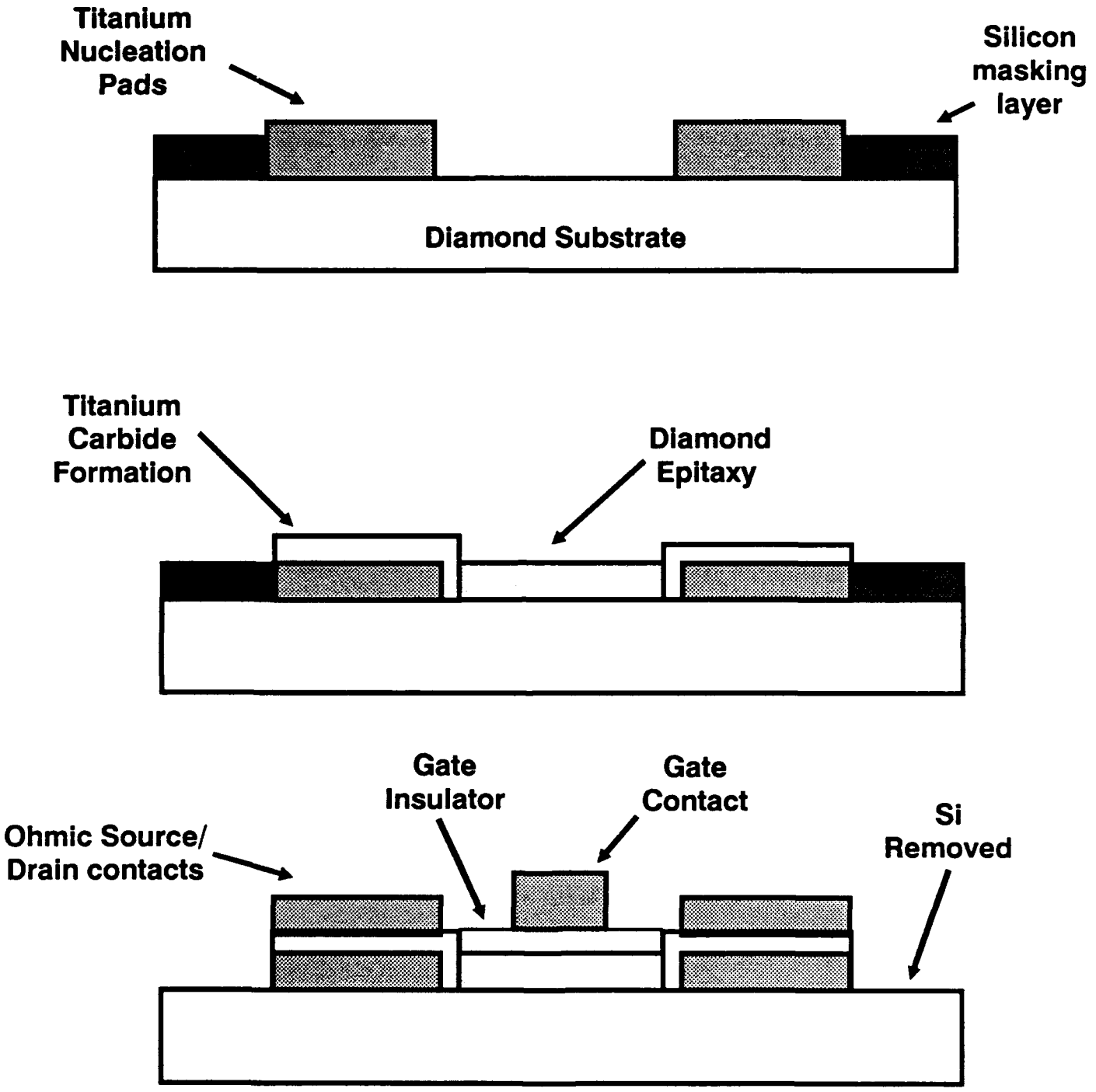

Figure 12. Schematic of a diamond FET device fabrication sequence using selective doped homoepitaxial deposition.

Potential n-type sources have been investigated again in this quarter. The sources evaluated were Li via a solid source of LiF and Na via a solid source of NaOH. Earlier Li doping results were reported in the third quarterly report for 1989. It was found that under diamond growth conditions both the LiF and NaOH are dissolved by the atomic hydrogen in the reactor. Li and Na emissions were observed in the reactor once the sources began to volatilize. Diamond deposition, with the sources present in the reactor, resulted in high incorporation of Li or Na into the samples ($> 10^{20}$ cm^3). Consequently, growths were performed with no source of Li or Na in the reactor other than the Li or Na residing on the chamber fixtures following "reactor dosing". Typically, a solid source would be introduced into the reactor, a discharge initiated, whereby emissions of Li or Na could be detected, the solid source removed, and the reactor deconditioned by a hydrogen discharge for some predetermined time before introducing a substrate for doped diamond deposition. More work was performed with Li doping as activated Na resulted in failure of vacuum feedthroughs after a few discharges containing NaOH. Homoepitaxial films doped with Li were p-type by Hall measurements. One such sample was sent to NOSC for metallization and electrical characterization. The carrier concentration at room temperature was $\sim 2.8\times10^{16}$cm^{-3}, p-type, with a mobility of $\sim$ 143 cm^2/V-sec. Variable temperature conductivity shows the activation energy, E_a, to be 0.23 eV. Figure 13 shows a plot of carrier concentration vs. reciprocal temperature. This is consistent with RTI results reported last year of $E_a = 0.25$ eV for Li doping. It should be noted that it has been verified that p-type conductivity is observed when Li is introduced in the manner described above. Interestingly, higher

mobilities have been obtained as compared to last year. We believe that there could be several factors that might contribute to this variability. Variations in Li concentration due to use of a solid-source for Li doping and/or the variable quality of the diamond substrates may be reasons for this variation. The sample is currently being analyzed by SIMS for Li and F concentrations in the film. No homoepitaxial growths with Na doping were attempted. Late this quarter, B_2H_6 was used as a p-type dopant source. Previous work with B_2H_6 in He had resulted in poor diamond deposition. This was a consequence of the substantial amount of He that was introduced into the reactor with the B_2H_6. He dilution of the hydrogen discharge degrades the quality of deposited diamond layers. This quarter two sources of B_2H_6 in H_2 were evaluated. Samples deposited with a 10 ppm source were not sufficiently doped. The resistance of the deposited layer was so high that it could not be distinguished electrically from the bulk diamond substrate. It is known that the stability of 10 ppm B_2H_6 sources is a dubious. Frequently, the actual B_2H_6 concentration in a 10 ppm source can be less than 1 ppm. A 1000 ppm B_2H_6 in H_2 source was installed on the reactor. A doped homoepitaxial layer was grown using:

15 sccm	1% CH_4 in H_2,
7.5 sccm	2% CO in H_2,
2 sccm	1000 ppm B_2H_6 in H_2,
5 Torr,	
800 ° C.	

Variable temperature conductivity and Hall measurements were made. At room temperature, a hole concentration of $10^{17}cm^{-3}$ was observed with a 20 cm^2/V-s hole mobility. The conductivity vs. temperature measurements revealed two activation

energies, 0.24 eV for temperatures $> 125\,^{\circ}$C and 0.006 eV for lower temperatures. Figure 14 shows the carrier concentration vs. reciprocal temperature. The low activation energy at low temperature is unusual and may be indicative of surface conduction between electrodes. SEM pictures of the surface show a rather unusual topography with very small nodular particles on an otherwise planar surface. The substrate used for this growth was one that had been used previously for Si overgrowth experiments. It is speculated that perhaps the recovery of the substrate left particulates on the surface leading to the growth of these nodular-type particles.

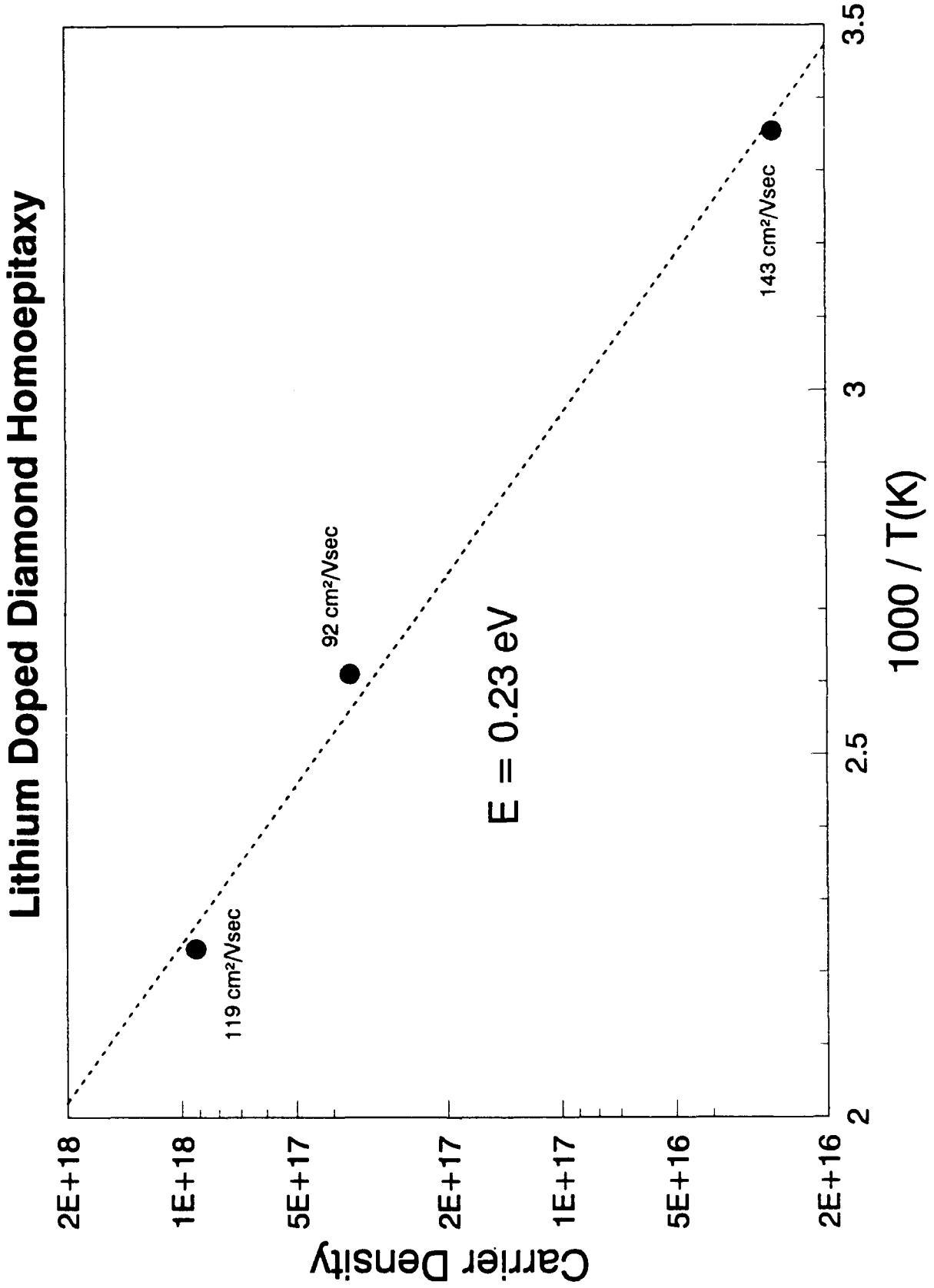

Figure 13. Carrier concentration vs. reciprocal temperature for a Li doped homoepitaxy. The activation energy was measured to be 0.23 eV for this p-type sample.

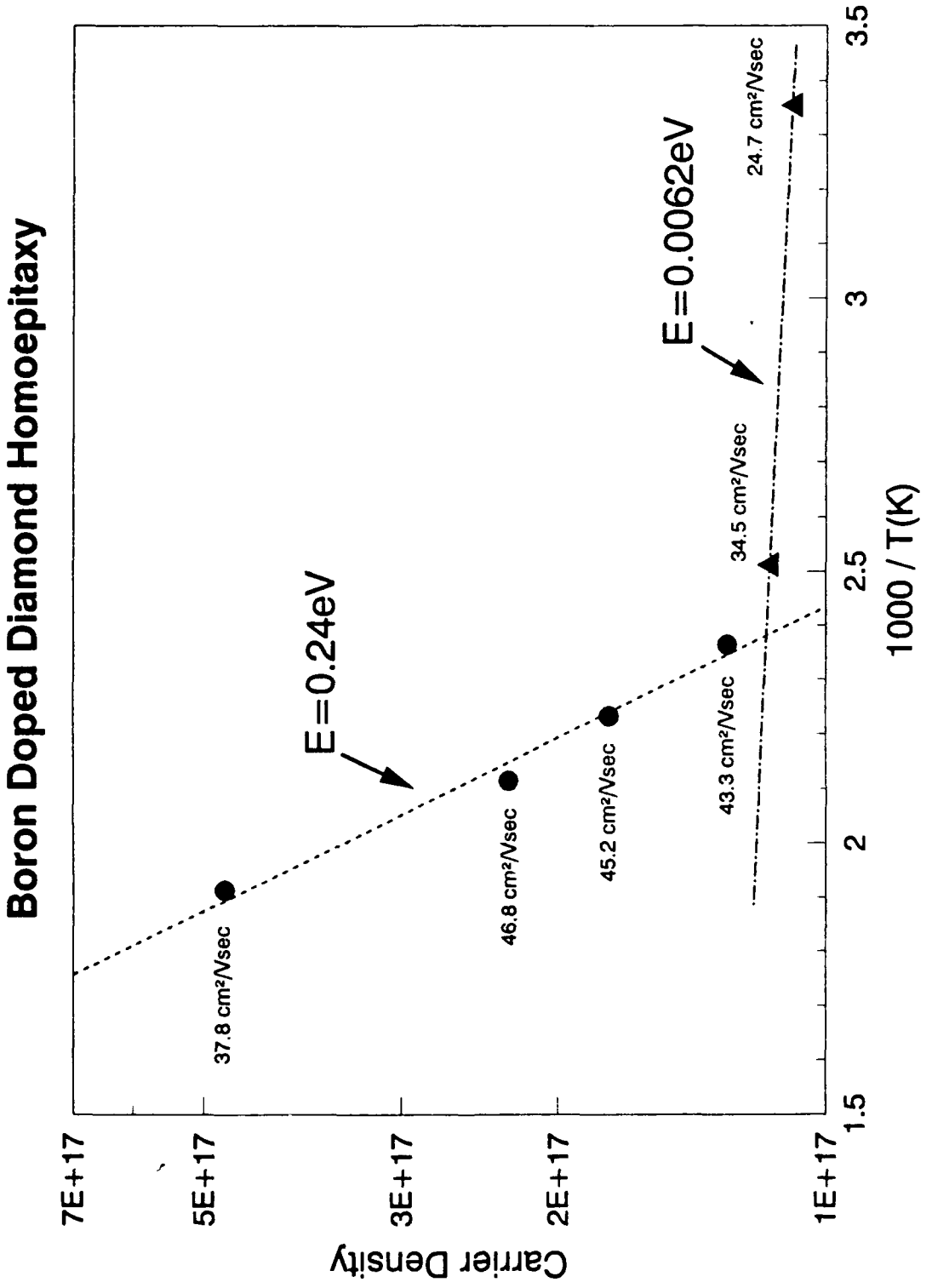

Figure 14. Carrier concentration vs. reciprocal temperature for a boron-doped homoepitaxial film.

5.0 Selective Diamond Growth and Overgrowth

Fabrication of the diamond device structure outlined in Section 4.0 depends on selective diamond nucleation. Given the difficulty in nucleating diamond on foreign substrates, selective diamond growth seems assured, provided the mask material does not dissolve in the atomic hydrogen ambient. More sophisticated device structures may require diamond overgrowth capability. To test selective nucleation, growth, and overgrowth, Si and Ni layers were deposited on natural type Ia substrates. The layers were MBE deposited by Dr. Trevor Humphreys at North Carolina State University. Si layers were $\sim$ 2000 Å thick; Ni layers were $\sim$ 400 Å thick. The Ni layers were single crystalline while the Si layers were polycrystalline or amorphous. The deposited layers were then photolithographically patterned so as to etch remove small areas of Si or Ni leaving holes in the mask. Thus, diamond was exposed upon which diamond growth would proceed and overgrow. The patterned substrates were introduced into the low pressure rf-plasma assisted CVD system for diamond deposition.

Results on the Ni patterned substrates are shown in Figure 15. The SEM photograph shows that a fairly smooth diamond layer had deposited in the diamond window. The area where the Ni existed prior to diamond deposition showed a very roughened topography. The deposition there did not resemble either homoepitaxial growths or polycrystalline growths on scratched surfaces. Micro-Raman results showed the area over the Ni to be diamond with a 5 cm^{-1} FWHM and some disordered carbon. Despite differences in topography between the areas where Ni had existed prior to diamond deposition and those areas where Ni had been chemically removed, Micro-Raman from

the area above the Ni window was identical to the diamond spectrum taken above the Ni regions. It seemed possible that the Ni mask (under conditions of diamond growth) had become discontinuous. Another Ni patterned sample was introduced into the diamond reactor for a limited time, $\sim$ 15 minutes. SEM analysis of that sample showed many regions extending from one diamond window to another with similar topography. It appears the Ni mask had separated allowing diamond on diamond homoepitaxial growth.

Experiments with Si masks were far more successful than with Ni masks. Figure 16 shows a plan view of the surface the Si patterned diamond substrate after growth. Notice that the diamond had grown above the Si mask. and that the Si mask did prevent substantial polycrystalline diamond nucleation. The topography of the overgrowth region does not appear to be as smooth as the diamond that grew over the center of the Si window. Many areas in front of the overgrowing diamond have nucleated diamond. This unwanted nucleation is incorporated as the overgrowth proceeds. This incorporation will likely produce defects in the overgrowth and result in poorer topography. Diamond areas not covered by Si had nucleated and grown homoepitaxially. The FWHM of Micro-Raman spectra was used to distinguish homoepitaxial growth from polycrystalline growth. FWHM of 2.5 - 3.0 cm^{-1} were seen in the homoepitaxial regions. FWHM of 5.0 - 6.0 cm^{-1} were seen in regions above the Si where polycrystalline diamond had nucleated. SEM examination showed that the diamond in the window areas had overgrown the Si pattern. This is suggested by the straight parallel diamond faces existing over the Si pads. This was confirmed by etch

removing the Si, Pt coating the sample to avoid charging in the SEM, and examining a cleaved cross-section area where the Si had been. Figure 17 shows one such region where the diamond had grown through the window and over the Si. The overgrowth appears approximately isotropic extending as far over the Si as it did above the Si.

Future work in overgrowth will evaluate other mask materials such as SiO_2, Si_3N_4, Ti, and W. (These are likely materials to be used in device fabrication.) Unlike the heterojunction studies, work here will focus on identifying a mask material upon which no spontaneous diamond nucleation occurs.

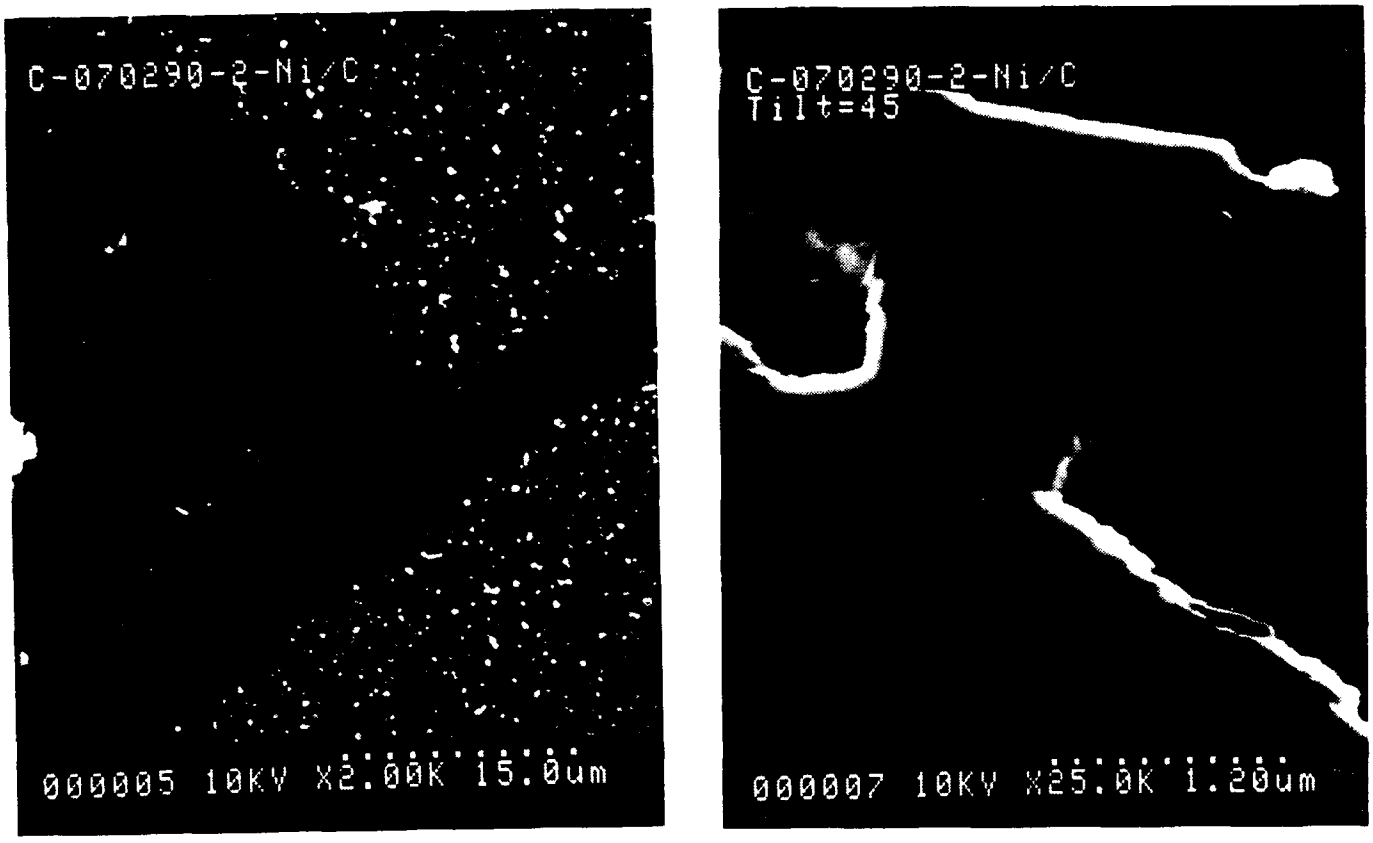

Figure 15. SEM micrograph of Ni patterned diamond substrate after diamond deposition.

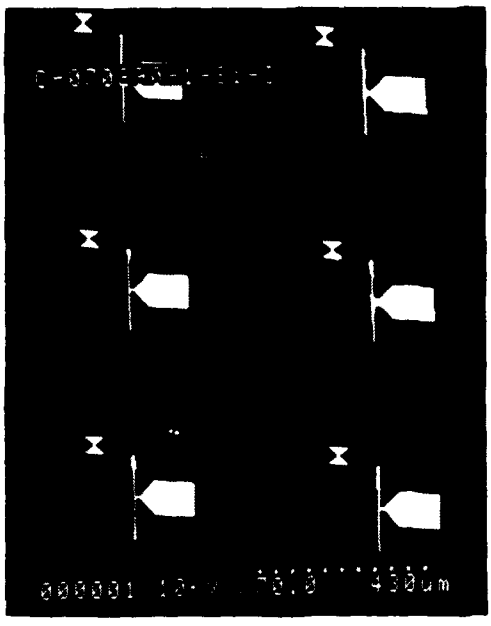

Pattern Used

Higher Magnification

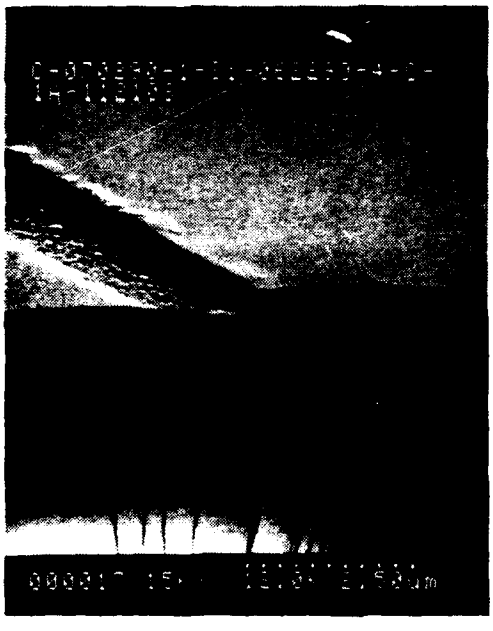

Cleaved Cross-Section

Figure 16. SEM micrograph of Si patterned diamond substrate after diamond deposition.

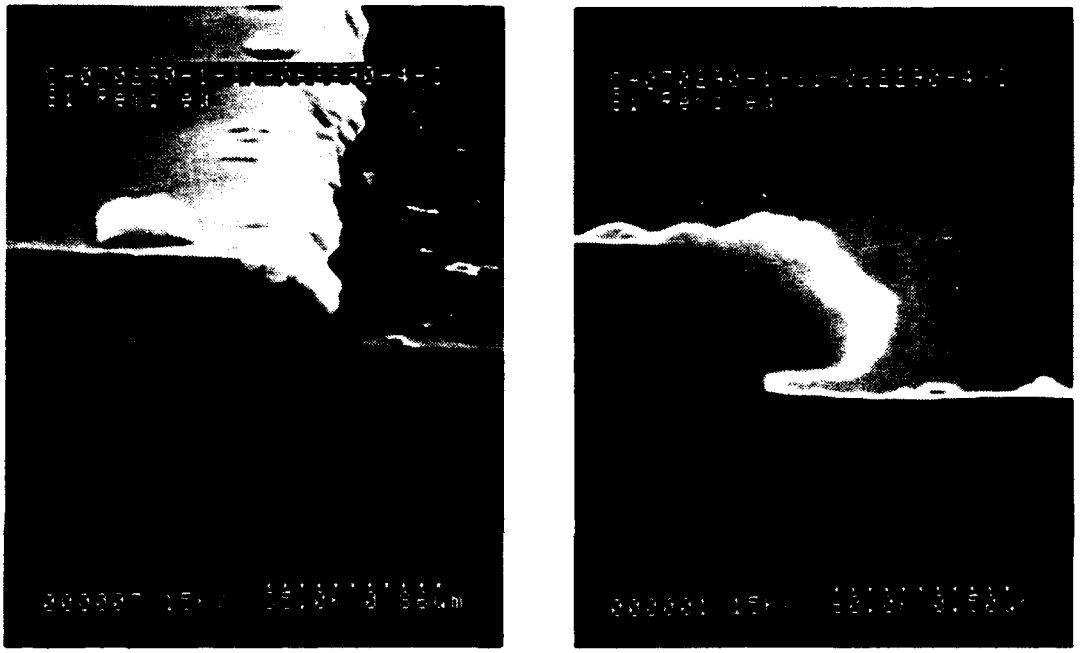

Figure 17. SEM of cleaved cross-section showing diamond epitaxial lateral overgrowth.

6.0 Current Directions

Demonstration of selective growth and overgrowth has certainly fostered many ideas to be investigated during the remainder of the year. Studies will investigate which materials or classes of materials will be preferable as a mask promoting overgrowth and eliminating nucleation on the mask. Investigation of overgrowth as a function of substrate temperature will be important in promoting enhancement of the lateral overgrowth. Device structures will be fabricated using selective growth to define the active device areas. Work is also underway to move the low-pressure rf-plasma assisted CVD system onto the vacuum transfer vessel. This should facilitate the investigation of interlayers on metal substrates for heteroepitaxial growth. Surface chemistry studies are targeting thermal desorption studies on diamond(100) surfaces and investigation of fluorocarbon gas/surface interactions.